FPN 2

EG&G INC.

TECHNICAL REPORT

NUMBER B-3147
EGG-1183-235
24 SEPTEMBER 1965

PROGRESS REPORT
IMPULSIVE LOAD TESTS
ON CYLINDRICAL ASSEMBLIES
PHASE 1

By

R. C. O'Rourke
C. B. Dobbie
S. Protopapa
L. E. Smollen
C. O. Phillips, Jr.
J. Z. Farber

For

The Sandia Corporation

1147/544

SYSTEMS DIVISION

EDGERTON, GERMESHAUSEN & GRIER, INC.

CONTENTS

LIST OF TABLES

LIST OF ILLUSTRATIONS

Page

SECTION I
INTRODUCTION

On June 16th, 1965, activities were initiated by the Advanced Research Department of Edgerton, Germeshausen & Grier, Inc. to perform impulsive load tests on aluminum cylinders as specified in a statement of work received from the Sandia Corporation, Livermore Laboratory. The general purpose of the tests was to demonstrate the impulsive load capabilities of pulsed magnetic coils and exploding films. Existing facilities at EG&G were to be used to demonstrate these capabilities at a minimum of time and cost. The following report presents an accounting of the test results as initially prepared for Sandia representatives during their visit to EG&G on the 15th and 16th of August 1965.

Section II which follows provides a discussion of the electrical and electronic aspects of the tests. Section III presents the results of analyses performed to determine failure predictions for the Sandia test cylinders, and Section IV discusses the various facets of the laboratory experiments which were conducted.

2.1 INTRODUCTION

Consider the LRC circuit shown in Figure 2.1. L(t) is the time-dependent inductance associated with a cylindrical structure which is placed inside a single-turn solenoid and subjected to a time dependent magnetic-pressure pulse, P(t). The parameters which characterize the EG&G pulsed power system illustrated in Section IV are:

$$C = 168\ \mu F$$

$$L_{ext} = 45 \text{ nanohenries}$$

$$\frac{1}{2} CV_o^2 = 33 \text{ kilojoules for } V_o = 20 \text{ kV}$$

Both the switch resistance, R_s, and the resistances of the solenoid system and workpiece are considered to be negligible. The solenoid is shown in Figure 2.2.

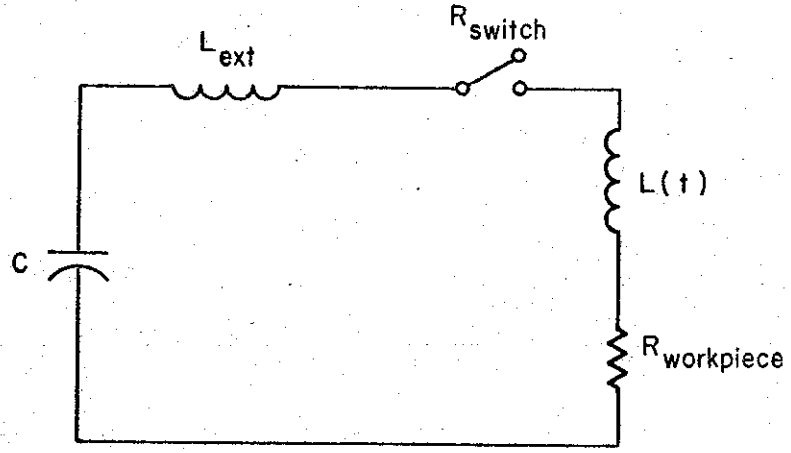

Figure 2.1 Schematic of the L(t), R, C circuit.

The thick-walled solenoid of the radius, R_c, is assumed to be rigid while the cylindrical structure radius, $R_M(t)$, can change in time.

The magnetic field generated in the region between the metal structure and the coil is given by the long solenoid formula

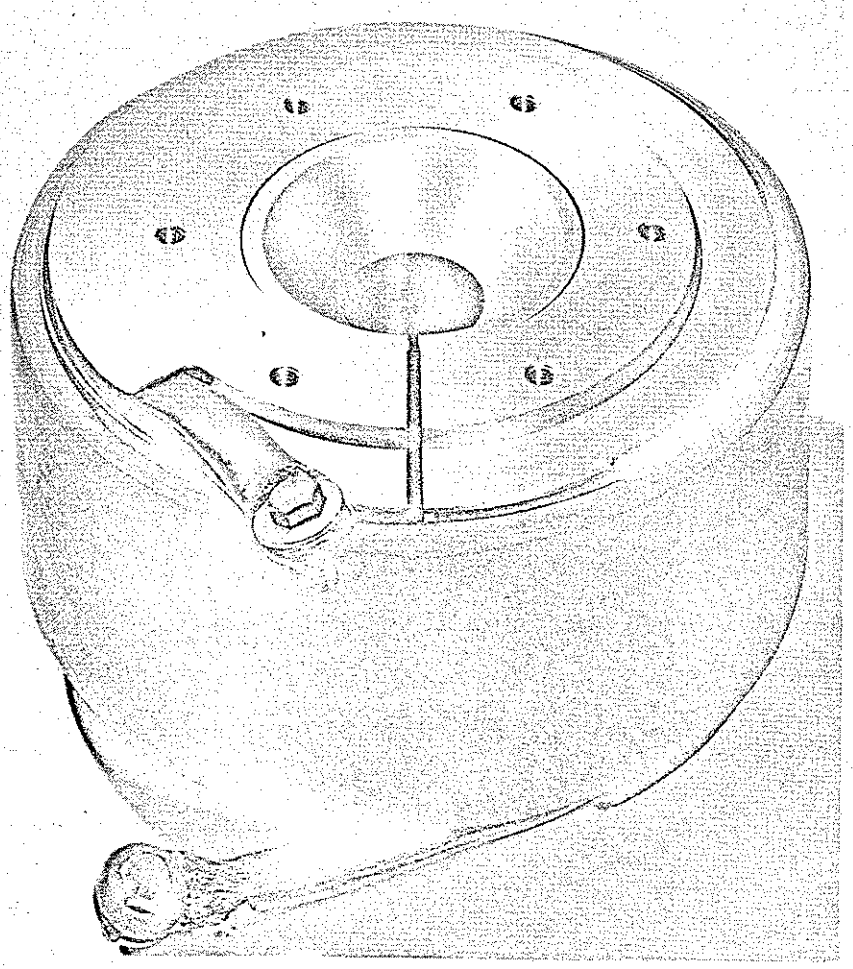

Figure 2. 2 Solenoid used with the EG&G pulsed power system.

$$B = \frac{4\pi I}{10 \ell} \quad \text{Gauss} \qquad (1)$$

where I is the solenoid current, in amperes

and ℓ is the axial length of the solenoid, in centimeters.

The magnetic pressure, (P_M) in dynes/cm^2, exerted on the structure is simply the energy density stored in the magnetic field and is given by

$$P_M = \frac{B^2}{8\pi} = \left(\frac{4\pi}{10\ell}\right)^2 \frac{I^2}{8\pi}$$

$$= \frac{2\pi}{\ell^2} I^2 \times 10^{-9} \quad \text{Atmos} \qquad (2)$$

One can measure the time-varying current, I(t), by using a very small pick-up loop, of area A_p, as a pick-up probe in the space between the solenoid and the workpiece. One has for the voltage, V_p, induced in this loop (ignoring polarity)

$$V_p = 10^{-8} A_p \frac{d}{dt} B$$

$$= 10^{-8} A_p \frac{4\pi}{10\ell} \frac{d}{dt} I \quad \text{volts} \qquad (3)$$

where A_p = area of loop, in cm^2.

Solving Equation (3) for I(t) gives

$$I(t) = \frac{10^9 \ell}{4\pi A_p} \int_o^t dt' \, V_p(t') \qquad (4)$$

and $P_M(t)$ can be obtained directly from this result by using Equation (2).

For the remainder of this report, all distances are measured in centimeters, all pressures in Atmos or psi are marked, all currents are given in amperes, all magnetic fields in Gauss and all voltages and potential in rationalized MKS Volts.

The external driving pressure, $P_M(t)$, causes the cylindrical structure to be compressed. In turn, this compression causes the cylinder radius, $R_M(t)$, to vary in time. One would like to design an electrical measurement technique, similar to a strain gauge, which will allow one to follow the circumferential average motion of $R_M(t)$ as the cylinder is compressed inwardly (not necessarily in a radially symmetrical manner if buckling occurs). To design the technique, one should first note that the load inductance, L(t), is a geometrical quantity which depends on the area of space existing between the coil and the cylindrical structure and, therefore, provides a measure of $R_M(t)$. Equating the total magnetic energy contained in the coil-cylinder interspace to the volume of energy stored in the inductance, L(t), one has

$$\frac{1}{2} L(t)\, I^2 = \frac{B^2}{8\pi}\, \pi\, (R_c^2 - R_M^2)\, \ell \times 10^{-7} \quad \text{joules} \tag{5}$$

where R_c is the solenoid radius, in cm.

Writing the magnetic field in terms of the current [from Equation (1)], one obtains

$$L(t) = \frac{4\pi^2}{\ell} \left[R_c^2 - R_M^2(t) \right] \quad \text{nanohenries} \tag{6}$$

If both the load voltage, V(t), across L(t) and the current, I(t), through the solenoid are measured, then from Faraday's Law one obtains

$$V(t) = \frac{d}{dt} \left[L(t)\, I(t) \right] \times 10^{-9} \quad \text{volts} \tag{7}$$

(polarity ignored), where it should be understood that L(t) must be defined by Equation (6). L(t) can be exposed in terms of the number of magnetic flux-linkages contained in the coil-cylinder interspace area using Equations (6) and (7).

Then

$$L(t) = \frac{4\pi^2}{\ell}\left[R_c^2 - R_M^2(t)\right] = \frac{\int_o^t dt'\ V(t')}{I(t)} \qquad (8)$$

and, expressing the current, I(t), in terms of the induced voltage across the pick-up loop, V_p, Equation (4), one has

$$\pi\left[R_c^2 - R_M^2(t)\right] = A_p \frac{\int_o^t dt'\ V(t')}{\int_o^t dt'\ V_p(t')} \qquad (9)$$

from which $R_M(t)$ and $\dot{R}_M(t)$ (which gives the velocity of the moving cylinder wall) can, in principle, be obtained. Note that this result is independent of the length of the solenoid. The velocity, $\dot{R}_M(t)$, can either be positive or negative depending on whether or not the cylinder is being compressed or expanded. The actual experimental measurement technique for accurately obtaining V_p (which gives I(t)) and V(t) (within ~ 1 percent) on a common time scale is yet to be developed, but should be possible.

One can also electrically measure the work being done on the cylindrical structure up to a given time, t, by examining the expression for the flow of energy into the solenoid.

$$E(t) = \int_o^t dt'\ I(t')\ V(t') = \int_o^t dt'\ I(t')\frac{d}{dt'}\left[L(t')\ I(t')\right]$$

$$= \frac{1}{2}LI^2\Big|_o^t + \frac{1}{2}\int_o^t dt'\ I^2(t')\frac{d}{dt'}L(t') \quad \text{joules} \qquad (10)$$

The first term in the expression represents the energy stored in the magnetic field. The second term, which occurs only because of the presence of the time-varying inductance, represents the work done on the cylindrical structure by the magnetic pressure. The interchange of energy between the magnetic field and the workpiece can be reversible for small strains or irreversible for permanent deformations.

Denoting the second term of Equation (10) by W_s, and recognizing that the inductance, $L(t)$, can be expressed in a completely general manner in terms of the magnetic flux, $\phi(t)$, by $L(t) = \frac{\phi(t)}{I(t)}$, one can write

$$W_s = \frac{1}{2} \int_0^t dt' \, I^2(t') \, \frac{d}{dt'} \, L(t')$$

$$= \frac{1}{2} \int_0^t dt' \, I^2(t') \, \frac{d}{dt'} \left(\frac{\phi(t')}{I(t')} \right)$$

$$= \frac{1}{2} \int_0^t dt \left(I \frac{d\phi}{dt} - \phi \frac{dI}{dt} \right)$$

$$= \frac{1}{2} \int_0^t dt \left(IV - \frac{d}{dt} (\phi I) + IV \right)$$

$$= \int_0^t dt \, I(t') \, V(t') - \frac{1}{2} \int_0^t dt' \, \frac{d}{dt'} (\phi I)$$

$$= \int_0^t dt' \, I(t') \, V(t') - \frac{1}{2} L(t) \, I^2(t) \qquad (11)$$

where repeated use has been made of Faraday's Law, $V = \frac{d\phi}{dt}$.

Then in Equation (11), by replacing L(t) in terms of I(t) and V(t) and using Equation (8), one obtains

$$W_s = \int_0^t dt' \, I(t') \, V(t') - \frac{1}{2} I(t) \int_0^t dt' \, V(t') \quad \text{joules} \tag{12}$$

Thus, one can obtain the work done by the magnetic pressure on the cylindrical workpiece simply by measuring both V(t), the voltage across the single-turn solenoid, and I(t), the current in the solenoid. By means of the above analysis, it has been shown that all of the quantities of interest, the time-varying inductance L(t), the workpiece radius $R_M(t)$ and its velocity of motion $\dot{R}_M(t)$, and the work done on the workpiece, $W_s(t)$, can all be expressed in terms of these two parameters. Therefore, one need measure only the voltage across the solenoid, V(t), and the corresponding voltage, V_p, across the current pick-up loop to obtain all of the pertinent information concerning this problem.

2.2 NUMERICAL ESTIMATES

To acquire a feeling for the magnitude of magnetic pressures and impulses available from the EG&G bank, it is interesting to consider an approximation where the total circuit inductance, L, is essentially constant with time

$$L = L_{ext} + L(t)$$

In most cases, L_{ext} is so much greater than L(t), that the assumption that L is constant is quite good, even though L(t) does vary somewhat with time. Such an approximation makes an accurate measurement of $R_M(t)$ virtually impossible, but nevertheless, is instructive in obtaining estimates of the magnetic pressure impulse.

For the general case of an RLC circuit with passive circuit elements, it is instructive to review the three classical cases.

2.2.1 Case 1, $R^2 < \frac{4L}{C}$ (Underdamped). This term characterizes a ringing circuit, so called because energy is continuously transported between the capacitor and the inductances at a rate determined by the ringing frequency

$$\omega = \sqrt{\frac{1}{LC} - \frac{R^2}{4L^2}} \tag{13}$$

The corresponding solution for the current is

$$I_1(t) = \frac{V_o}{\omega L} e^{-at} \sin \omega t \tag{14}$$

where

$$a = \frac{R}{2L} \tag{15}$$

The peak current occurs at

$$I_{max} = \frac{1}{\omega} \tan^{-1} \frac{\omega}{a} \tag{16}$$

and is given by

$$I_1^{peak} = I(t_{max}) = V_o \sqrt{\frac{C}{L}} e^{-at_{max}} \tag{17}$$

2.2.2 Case 2, $R^2 > \frac{4L}{C}$ (Overdamped). This term characterizes the overdamped circuit. The current in this circuit does not exhibit the oscillatory behavior of a damped exponential and is given by

$$I_2(t) = \frac{V_o}{KL} e^{-at} \sinh Kt \tag{18}$$

where

$$K^2 = \left(\frac{R^2}{4L^2} - \frac{1}{LC} \right) \tag{19}$$

This current reaches a maximum value at time

$$t_{max} = \frac{1}{K} \tanh^{-1} \frac{K}{a} \tag{20}$$

which yields

$$I_2^{peak} = I_2(t_{max}) = V_o \sqrt{\frac{C}{L}} \; e^{-at_{max}} \tag{21}$$

2.2.3 Case 3, $R^2 = \frac{4L}{C}$ (Critically Damped). This set of conditions characterizes the critically damped circuit and denotes a balance between the resistive and reactive components of the total circuit impedance.

The solution for this case is

$$I_3(t) = \frac{V_o}{L} \; t \, e^{-at} \tag{22}$$

with

$$t_{max} = \frac{2L}{R} = \frac{1}{a} \tag{23}$$

and

$$I_3^{peak} = I_3(t_{max}) = 2 \frac{V_o}{R} \; e^{-1} \tag{24}$$

where

e is the base of the Naperian logarithm.

These three different solutions are clearly illustrated in Figure 2.3 which is a plot of I(t) versus time for all three cases. Numerical values were obtained by taking C = 168 μF which corresponds to the capacitance of the bank, V_o = 20 kV and L = 60 nH. (Since L_{ext} = 45 nH, this corresponds

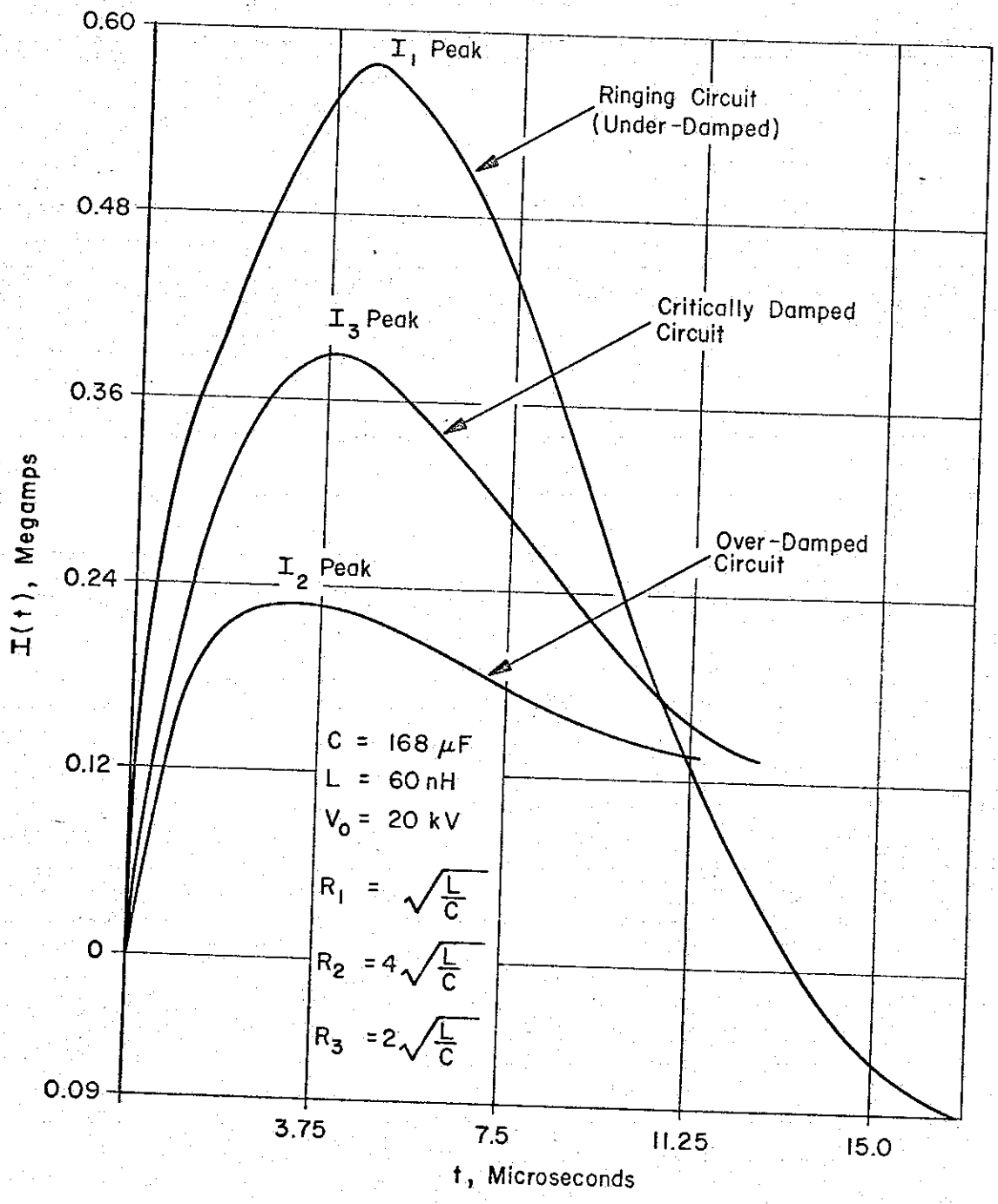

Figure 2. 3 Plots of current vs time for the underdamped, overdamped, and critically damped LRC circuit.

to a load inductance of 15 nH and satisfies the criterion $L(t) < L_{ext}$.) It was assumed that the switch resistance could be varied to satisfy the conditions for the three different cases.

CASE 1 - R was set equal to $\sqrt{\frac{L}{C}}$ which is one-half of the critical damping resistance. The ringing frequency for this case is 36.6 kHz. The maximum current of 580,000 amperes occurs at 4.5 μsec, and the current reverses polarity at 13.5 μsec.

CASE 2 - R was chosen to equal $4\sqrt{\frac{L}{C}}$ which is twice critical damping. The maximum current of 228,000 amperes occurs at 2.85 μsec for this case.

CASE 3 - Here, one must choose $R = 2\sqrt{\frac{L}{C}}$, the critically damped criterion. The maximum current of 390,000 amperes occurs at $t = 3.75$ μsec.

One can readily observe from Figure 2.3 that the maximum peak current is obtained in the underdamped case.

For the case of a completely undamped circuit, $R = 0$

$$I_o^{peak} = V_o \sqrt{\frac{C}{L}} \tag{25}$$

Comparing this undamped value with the peak current for the critically damped case, one finds

$$\frac{I_3^{peak}}{I_o^{peak}} = e^{-1} \tag{26}$$

If the ringing circuit were completely undamped, one would find a ringing frequency of 42.5 kHz and a peak current of 1.06 megamps.

Thus, the maximum current for the critically damped circuit is a factor of e less than the maximum undamped current. The maximum magnetic pressure in the critically damped circuit is, accordingly, a factor of e^2 less than the corresponding quantity for the undamped circuit.

2.3 DETERMINATION OF THE MAGNETIC PRESSURE IMPULSE

A single quantity which provides a good measure of the capability of the capacitor-bank system to perform work on the cylindrical workpiece is the magnetic pressure impulse, the time-integrated magnetic pressure. In general, one can write

$$\Gamma = \frac{1}{8\pi}\left(\frac{4\pi}{10\ell}\right)^2 \int_0^\infty dt\, I^2(t) \quad \text{atmos-}\mu\text{sec} \tag{27}$$

To properly approach this subject, it is necessary to consider separately the three different circuit conditions.

2.3.1 Case 1 - Underdamped Circuit. The current for the ringing circuit has been previously derived and is given by Equation (14). Substituting this quantity in the above expression, one obtains

$$\Gamma = \frac{2\pi}{100\ell^2}\left(\frac{V_o}{\omega L}\right)^2 \int_0^\infty dt\, e^{-2at} \sin^2\omega t$$

$$= \frac{\pi}{50\ell^2}\left(\frac{V_o}{L}\right)^2 \frac{1}{4a}\,\frac{1}{a^2+\omega^2} \quad \text{atmos-}\mu\text{sec} \tag{28}$$

However, from the definitions of ω and a, one finds

$$\frac{1}{4a}\,\frac{1}{a^2+\omega^2} = \frac{L^2C}{2R} \tag{29}$$

so that

$$\Gamma = \frac{0.46\ E_o}{\ell^2\ La} \quad \text{psi-}\mu\text{sec} \tag{30}$$

where $E_o = \frac{1}{2} CV_o^2$ is the total bank energy, and $a = \frac{R}{2L}$.

2.3.2 Case 2 - Overdamped Circuit. The current for the overdamped circuit is given by Equation (18). Again, following the procedure outlined above, one obtains for the impulse,

$$\Gamma = \frac{0.46\ E_o}{\ell^2\ La}$$

which is identical to the expression obtained for the underdamped circuit.

2.3.3 Case 3 - Critically Damped Circuit. Although the current for the critically damped case is linear in time and the resulting integrals are different, the final expression for the impulse again is the same as was derived above. One finds

$$\Gamma = \frac{\pi}{50\ell^2}\left(\frac{V_o}{L}\right)^2 \int_o^\infty dt\ t^2\ e^{-2at}$$

$$= \frac{\pi}{50\ell^2}\ \frac{V_o^2}{R^2 a} \quad \text{atmos-}\mu\text{sec} \tag{31}$$

However, making use of the identity $R^2 = 4\ \frac{L}{C}$, one again obtains

$$\Gamma = \frac{0.46\ E_o}{\ell^2 La} \quad \text{psi-}\mu\text{sec} \tag{32}$$

Since the expression for the magnetic pressure impulse Γ is the same for all three cases, it follows therefore, that this result is independent of the particular relationship satisfied by the circuit elements L, R, and C and is derivable directly from the differential equation for the current, I(t). This can easily be demonstrated as is shown below.

Starting with the differential equation

$$L\frac{dI}{dt} + IR + \frac{1}{C}\int_o^t I(t')\,dt' = V_o \tag{33}$$

together with the initial condition

$$L\left(\frac{dI}{dt}\right)_o = V_o \tag{34}$$

One first differentiates with respect to time, giving

$$L\frac{d^2I}{dt^2} + R\frac{dI}{dt} + \frac{I}{C} = 0 \tag{35}$$

Multiplying each term by I(t) and integrating over all time, one obtains

$$L\int_o^\infty I\frac{d^2I}{dt^2}\,dt + \frac{1}{C}\int_o^\infty I^2 dt = 0 \tag{36}$$

The second integral in this expression is the quantity of interest since it is proportional to the impulse. The first term can easily be integrated by parts so that one obtains

$$\int_0^\infty I^2 dt = LC \int_0^\infty \left(\frac{dI}{dt} \right)^2 dt \tag{37}$$

This last integral can easily be evaluated. Returning to Equation (35), one now multiplies by $\frac{dI}{dt}$ and integrates. The result is

$$L \int_0^\infty \frac{dI}{dt} \frac{d^2I}{dt^2} dt + R \int_0^\infty \left(\frac{dI}{dt} \right)^2 dt = 0 \tag{38}$$

But

$$\int_0^\infty \frac{dI}{dt} \frac{d^2I}{dt^2} dt = -\frac{1}{2} \left(\frac{dI}{dt} \right)_0^2 = -\frac{1}{2} \frac{V_o^2}{L^2} \tag{39}$$

from the initial condition, Equation (34), so that

$$\int_0^\infty \left(\frac{dI}{dt} \right)^2 dt = \frac{1}{2} \frac{V_o^2}{RL} \tag{40}$$

Substituting this last result in Equation (37), one finally obtains

$$\int_0^\infty I^2 dt = LC \int_0^\infty \left(\frac{dI}{dt} \right)^2 dt = \frac{1}{2} C \frac{V_o^2}{R} = \frac{E_o}{R}$$

$R \int I dt = E_o$, conservation!

(41)

which leads directly to the previous result, Equation (32),

$$\Gamma = \frac{1}{8\pi} \int_0^\infty B^2 dt = \frac{\pi}{50 \ell^2} \int_0^\infty I^2 dt \quad \text{atmos-}\mu\text{sec}$$

$$= \frac{0.46}{\ell^2} \frac{E_o}{La} \quad \text{psi-}\mu\text{sec}$$

2.4 PRESSURE AND ENERGY CONSIDERATIONS

As a final example, consider a critically-damped L(t) RC circuit which contains the EG&G capacitor bank in series with an inductive load comprised of the coil-cylinder ensemble discussed above. Critical damping can be achieved by including a suitable resistance in the circuit. From Equation (24), one has for the critically damped case

$$I_3^{peak} = e^{-1} V_o \sqrt{\frac{C}{L}}$$

where $L = L_{ext} + L(t)$

and one can then write for the peak magnetic pressure (using Equation (2)

$$P_{max} = \left(\frac{B^2}{8\pi}\right)_{max} = \frac{\pi C V_o^2}{360 \ell^2} \frac{1}{\left[L_{ext}(nh) + \frac{4\pi^2}{\ell}(R_C^2 - R_M^2)\right] \times 10^{-9}} \text{ dynes/cm}^2 \qquad (42)$$

where L(t) has been expressed in terms of the solenoid-workpiece geometry as was previously shown in Equation (6). For the small strains of interest here, one can use the approximation

$$R_C - R_M = \Delta \; ; \; R_C + R_M \approx 2 R_M$$

so that Equation (42) can be rewritten

$$P_{max} \cong \frac{2.8\pi C V_o^2}{\ell} \frac{1}{\left[L_{ext}(nh) + 4\pi^2 \frac{2R_M}{\ell} \Delta\right]} \text{ atmospheres} \qquad (43)$$

For the EG&G bank, one has $C = 168\ \mu F$, $V_o = 20$ kV, $L_{ext} = 45$ nH

so that

$$P_{max} = \frac{5.9 \times 10^5}{\ell} \left[\frac{1}{45 + 40 \frac{2R_M}{\ell} \Delta} \right] \text{ atmospheres} \quad (44)$$

This peak magnetic pressure occurs at time

$$t_{max} = \sqrt{CL} \cong 4 \times 10^{-7} \left[45 + 40 \left(\frac{2R_M}{\ell} \right) \Delta \right]^{1/2} \text{ seconds} \quad (45)$$

The maximum energy stored in the magnetic field is given by

$$E_{max} = \frac{1}{2} L(t) I_{max}^2$$

$$\cong \frac{4500 \Delta \left(\frac{2R_M}{\ell} \right)}{1 + \Delta \left(\frac{2R_M}{\ell} \right)} \text{ joules} \quad (46)$$

To simulate uniform impulse loading of cylindrical structures, one requires that the solenoidal length be at least equal in magnitude to the diameter of the cylindrical structure. It can be shown that for the case of $\ell = 2R_M$, the maximum variation in the axial magnetic field at all points on the cylinder surface is less than 12 percent.[1] Typical experiments conducted at the EG&G facility used solenoids of lengths nearly equal to the initial outer diameter of the Sandia cylinder being tested. A solenoid 7 cm in length was used in conjunction with Sandia Test Cylinders 6.35 cm to 7.62 cm in diameter (2.5 to 3.0 inches).

Choosing $2R_M = \ell$ modifies the expressions for E_{max}, P_{max}, and t_{max} to read

$$E_{max} \sim 4500 \frac{\Delta}{1+\Delta} \quad \text{joules} \tag{47}$$

$$P_{max} \sim \frac{1.5 \times 10^4}{\ell} \frac{1}{1+\Delta} \quad \text{atmos} \tag{48}$$

$$t_{max} \sim 2.7 \ (1+\Delta)^{1/2} \quad \mu\text{sec} \tag{49}$$

One can readily see from Equations (47) and (48) that an increase in Δ produces a decrease in the maximum value of the magnetic pressure, whereas the converse is true as regards the maximum energy stored in the magnetic field. This is consistent with the fact that an increase in Δ increases the solenoid-workpiece interspace volume and thus causes the magnetic-volume energy density, or pressure, to decrease. On the other hand, the energy which is delivered to the solenoid is very roughly a measure of the ratio of the solenoid-workpiece inductance to the total inductance of the circuit. Since the former is linear in Δ, this ratio increases as the solenoid-workpiece spacing is widened. Typical values of Δ ranged from 0.08 cm to 0.5 cm for the various experimental tests conducted. From Equations (47), (48), and (49), and corresponding ranges of values of E_{max}, P_{max}, and t_{max}, respectively, one finds

$$E_{max} \sim 333 \text{ to } 1500 \quad \text{joules}$$

$$P_{max} \sim 2000 \text{ to } 1430 \quad \text{atmos}$$

$$t_{max} \sim 2.8 \text{ to } 3.4 \quad \mu\text{sec}$$

2.5 PROPOSED PROGRAM OF STUDY

It has been asserted that much useful and significant information could be obtained from an experiment involving impulsive loading of a cylindrical workpiece if one could simultaneously measure both the voltage, V(t), across the load and the current, I(t), in the circuit. Another section of this report discusses the problems in experimental procedure which are inherent to such an undertaking. Assuming that these measurements can be achieved without dwelling further on the methods and techniques to be used, one must next discuss the manner in which these experimental results are to be analyzed and put to optimum use. From the time-history traces of current and voltage, one can then obtain a) the time-integrated voltage, b) the rate of change of current, c) the time-integrated power.

Then, as was previously shown in Equation (7), one can directly obtain the time-varying inductance

$$L(t) = \frac{\int_0^t dt' \, V(t')}{I(t)} \tag{50}$$

and this quantity can then be related to $R_M(t)$, the time-dependent boundary of the cylindrical workpiece, by

$$R_M(t) = \left(R_C^2 - \frac{\ell L(t)}{4\pi^2} \right)^{1/2} \tag{51}$$

This expression gives only the average value of $R_M(t)$ at any given time since, in relating the inductance to R_M in this manner, one tacitly assumes that the buckling cylinder always maintains a circular cross-section. In actuality, the action of the magnetic pressure pulse will distort the cylinder.

and the distance of the outer boundary from the center, at any given instant of time, will differ from position to position. One can photograph the motion of the cylinder and compare this result with the average value of $R_M(t)$ given by Equation (51). Of special interest should be a comparison of the actual and predicted final position of the cylinder.

The approximate inward velocity of the cylinder can also be determined by differentiating Equation (51).

$$\dot{R}_M(t) = - \frac{\ell}{8\pi^2} \frac{d}{dt} L(t) \frac{1}{\left(R_C^2 - \frac{\ell L(t)}{4\pi^2} \right)^{1/2}} \qquad (52)$$

The time rate of change of L can easily be obtained from the original electrical measurements. From the expression for the voltage drop across an inductance [Equation (50)], one has

$$\frac{d}{dt} L(t) = \frac{1}{I(t)} \left[V(t) - L(t) \frac{dI}{dt} \right]$$

$$= \frac{V(t)}{I(t)} - \frac{\int_o^t V(t')\, dt'}{I^2(t)} \frac{dI}{dt} \qquad (53)$$

The work done on the structure, as a function of time, can also be determined. From the expression developed earlier, Equation (11), one has

$$W_S(t) = \int_o^t dt'\, I(t')\, V(t') - \frac{1}{2} I(t) \int_o^t dt'\, V(t') \qquad (54)$$

Both the magnetic pressure, $P_M(t)$, and its time-integrated companion the magnetic pressure impulse, I, are easily obtainable solely from the current I(t).

2.6 COMPARISON OF SIMPLIFIED THEORY WITH EXPERIMENTAL RESULTS

Another section of this report which is concerned with Failure Predictions, discusses the various types of buckling which can occur when the Sandia Test Cylinders are subjected to short-duration pressure pulses. Values are given for the critical stress yields of a given cylinder under each of several possible buckling modes. A numerical estimate of the dynamic stress yield applied to a given cylinder by the magnetic pressure pulse can be obtained by judicious use of the above expressions for L(t) and $W_s(t)$. As a final exercise, the dynamic stress yield will be calculated and the results compared with the corresponding value of the critical stress for consistency.

In the absence of any experimental data, one can initially make some reasonable assumptions concerning the explicit time-variance of the coil-cylinder inductance, L(t). If one assumes that the cylinder boundary, $R_M(t)$, is uniformly accelerated from rest to some final velocity, $\dot{R}_M(t) = v_f$, then one can write

$$R_M(t) = R_M(0) - \frac{1}{2}\alpha' t^2 \tag{55}$$

Then, using the relationship between $R_M(t)$ and L(t), one has

$$L(t) = L_o + \alpha t^2 \tag{56}$$

where $L_o = \frac{4\pi^2}{\ell} [R_C^2 - R_M^2(0)]$ is the zero time inductance,

$$\alpha = \frac{4\pi^2}{\ell} \alpha' R_M(0) \times 10^9 \quad \text{nanohenries/cm}^2 \qquad (57)$$

and an additional term proportional to $\alpha^2 t^4$ has been neglected. As was mentioned elsewhere, the behavior of $\frac{dL}{dt}$ determines the work being done on the cylinder. One can write the expression for W_s in the form [Equation (10)]

$$W_s = \frac{1}{2} \int_o^\infty dt \; I^2(t) \; \frac{d}{dt} \; L(t) \qquad (58)$$

The time-derivative of the inductance is easily obtained from Equation (56) to give

$$W_s = \alpha \int_o^\infty t^2 \; I^2(t) \; dt \qquad (59)$$

Now, consider an experiment using a Sandia Test Cylinder placed inside a single turn coil connected in series with the EG&G pulsed power facility described above. Assume, furthermore, that the circuit is operated in the underdamped (ringing) condition to supply maximum stress to the cylindrical structure.

For $L_o < L_{ext} = 45$ nH, one can use the solution for I(t) in a constant LRC underdamped circuit; i. e. ,

$$I(t) = \frac{V_o}{\omega L} e^{-at} \sin \omega t$$

$$L = L_{ext} + L_o$$

$$a = \frac{R}{2L}$$

$$\omega = \left(\frac{1}{LC} - \frac{R^2}{4L^2}\right)^{1/2}$$

Using this expression for the current, one has, for the work done on the cylinder,

$$W_s = \frac{\alpha V_o^2}{\omega^2 L^2} \int_o^\infty t^2 e^{-2at} \sin^2 \omega t \, dt$$

$$= -\frac{1}{8} \frac{\alpha V_o^2}{L^2 \omega} \frac{d}{da} \left(\frac{1}{a} \frac{1}{a^2 + \omega^2}\right) \tag{60}$$

Rewriting a and ω in terms of the circuit elements leads to

$$W_s = \frac{\alpha E_o}{2R^2} (2L + CR^2) \tag{61}$$

where again

$$E_o = \frac{1}{2} CV_o^2$$

The work done on the cylinder represents a percentage of the capacitor band energy E_o and can also be written in the form

$$W_s = \eta E_o \tag{62}$$

where η represents the efficiency between energy stored in the bank and work done on the workpiece.

Equating these two expressions for W_s [Equation (61)], one can obtain the efficiency as a function of α which is a measure of the time rate of change of inductance according to

$$\eta = \frac{\alpha(2L + CR^2)}{2R^2} \tag{63}$$

In an actual experiment performed at the EG&G facility, an aluminum cylinder of initial radius $R_M(0) = 3.47$ cm, and wall thickness $h = 0.63$ cm, was placed in a coil of inner radius 3.832 cm, and length 7.0 cm, and connected to the EG&G pulsed power supply.

One has

$$R_c = 3.832 \text{ cm}$$

$$R_M(0) = 3.47 \text{ cm}$$

$$\ell = 7.0 \text{ cm}$$

$$L_o = 15 \text{ nH}$$

$$C = 168 \ \mu\text{F}$$

$$L_{ext} = 45 \text{ nH}$$

$$L = L_{ext} + L_o = 60 \text{ nH}$$

The circuit was observed to ring at a frequency of 50 kilohertz which corresponds to $\omega = 3.14 \times 10^5 \text{ sec}^{-1}$. From Equation (13) involving ω and the damping rate, a, one finds for the circuit resistance,

$$R = 0.003 \text{ ohms.}$$

The test cylinder was found to have undergone uniform circumferential plastic deformation as a result of the application of the magnetic pressure pulse. The cylinder radius was compressed from its initial value of 3.47 cm

to a final value of $R_M(f) = 3.40$ cm. This corresponds to a final inductance of 16.5 nanohenries which represents a change in inductance, ΔL, of 1.5 nanohenries. This change in inductance can be equated directly to the parameter α.

From Equation (56), one has

$$\Delta L = L(t) - L_o = \alpha t^2 . \qquad (64)$$

Previous analysis of the ringing circuit revealed that nearly all of the magnetic pressure impulse is supplied to the workpiece during the first half-cycle. Therefore, choosing $t = \frac{\pi}{\omega} = 10\ \mu$sec, one finds

$$\alpha = 15 \text{ henries/sec}^2$$

and thus, from Equation (63) a corresponding efficiency of

$$\eta = 10 \text{ percent.}$$

This value is in excellent agreement with those statements (see Section III) which indicate that typical efficiencies to be expected with the EG&G pulsed power facility are of the order of 10 percent.

With α known, one can next solve for the assumed uniform acceleration α' of the workpiece using the relationship

$$\alpha = \frac{4\pi^2}{\ell} R_M(0)\, \alpha' \times 10^{-9} \qquad (65)$$

and obtain

$$\alpha' = 7.8 \times 10^8 \text{ cm/sec}^2$$

The final velocity of the cylinder, v_f, is then given by

$$v_f = \alpha' t \tag{66}$$

and for $t = 10\ \mu$sec, one finds

$$v_f = 7.8 \times 10^3 \text{ cm/sec}$$

In Section III, Failure Predictions, it was concluded from an analysis of the elastic properties of the Sandia Test Cylinders that final velocities should not exceed 750 ft/sec (2.3×10^4 cm/sec). Note that this limiting value is indeed considerably greater than the value of v_f obtained immediately above.

With v_f known, one can now determine the momentum per unit area of the cylinder and equate this to the impulse Γ. One can then compare this value with that obtained from the integrated time average magnetic pressure.

Therefore, let $\Gamma_1 = mv = \rho h v$ represent the impulse computed from momentum considerations where $v = 7.8 \times 10^3$ cm/sec as was previously determined, $m = \rho h$ ($\rho = 2.7$ gm/cm^3) is the cylinder mass per unit area and $h = 0.63$ cm is the cylinder wall-thickness.

One finds

$$\Gamma_1 = 1.33 \times 10^4 \text{ atmos-}\mu\text{sec} - 2.0 \times 10^5 \text{ psi-}\mu\text{sec}$$

Using Equation (52), one obtains the impulse directly from the magnetic pressure. Denoting this quantity by Γ_2,

$$\Gamma_2 = \frac{0.46\ E_o}{\ell^2\ R/2} \sim 2.0 \times 10^5 \text{ psi-}\mu\text{sec} \tag{67}$$

Note that Γ_1 and Γ_2 which were calculated using widely diversified methods are in excellent agreement with each other.

Taking $\Gamma = 2 \times 10^5$ psi-μsec, and assuming that the impulse acts over 10 μsec, one has for the dynamic yield stress applied to the cylinder

$$P_M = 20,000 \text{ psi}$$

This value is below the 58,000 psi threshold required for excitation of any of the high order inelastic buckling modes for a cylinder with $a/h = 5.5$ as shown in Figure 2.3 in the section on Failure Predictions. In the actual experiment performed, the aluminum cylinder did not buckle but suffered uniform plastic deformation, as elsewhere mentioned, thus supporting the contention that the impulse was of insufficient magnitude to excite any of the high order inelastic buckling modes. Since the impulse is inversely proportional to the square of the length, the dynamic yield stress supplied by the EG&G capacitor bank can be increased by using cylindrical structures of shorter lengths.

(1) Reference on page 19 is:

Snyder, A. W., Fields of Finite Cylindrical Coils. Sylvania Electronic Systems, Applied Research Laboratory, Waltham, Massachusetts. Research Report No. 436 (to be published).

3.1 GENERAL

This Section presents the results of some approximate analyses which seek to establish the types of failure as well as the pressures and energy levels required to produce failure in the Sandia test cylinders. The analysis is approximate; the results obtained are meant to be used only as guides for designing experiments and for interpreting test data.

3.2 TYPES OF FAILURE

There are essentially two basic types of failure which may occur in cylinders subjected to external pressure, the first of which is failure by uniform circumferential plastic deformation. The second is failure due to buckling. Buckling may be purely elastic, may occur between the proportional limit and yield point, or may occur inelastically after considerable post-yield, plastic deformation. In the latter case, the failure must be viewed as a combined failure in which significant uniform, inelastic deformation is followed by inelastic buckling.

3.2.1 Uniform Plastic Deformation. The first and, as will be subsequently shown, predominant mode of failure for the Sandia A cylinders is by means of uniform circumferential plastic deformation (see Figure 3.1).

This type of failure, rather than the buckling type, will occur if the critical buckling stress of the cylinder in a probable buckling mode is greater than or equal to the dynamic yield stress. Section 3.2.2 provides a more detailed discussion of the possibility of buckling and the type of buckling (elastic or plastic) which might occur.

3.2.2 Elastic and Inelastic Buckling. A buckling failure (elastic or inelastic) can occur in any one of "n" modes as shown in Figure 3.2.

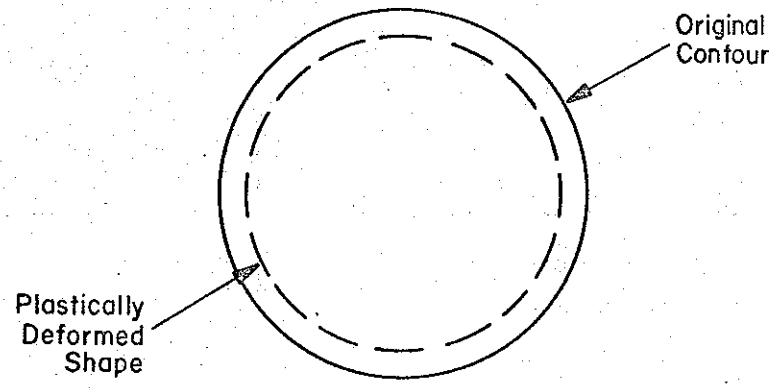

Figure 3. 1 Uniform circumferential plastic deformation.

The nature of the loading constraints determines the particular order of buckling mode obtained. For short duration pulse-type pressures, the constraints are such that buckling in the lower modes is precluded. On the basis of experimental magnetic forming data, it seems unlikely that buckling will occur in modes corresponding to $n < 8$.

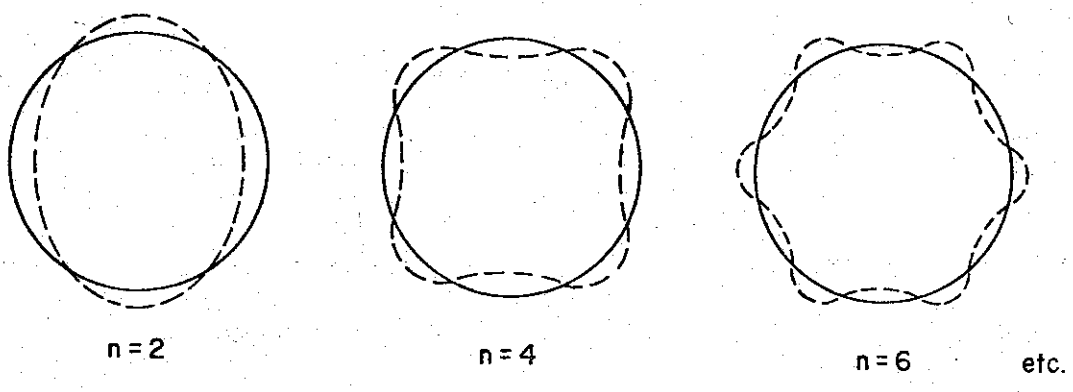

Figure 3. 2 Buckling modes.

For the purpose of discussing buckling phenomena, the stress-strain curve of 6061 T-6 Aluminum will be idealized as shown in Figure 3.3. To allow for dynamic strain-rate effects, the usual proportional limit yield and ultimate stress values have been multiplied by 1.6.[1] The value of the tangent modulus, E_t, in the inelastic range has been approximated from stress-strain data for Aluminum 6061 T-6.

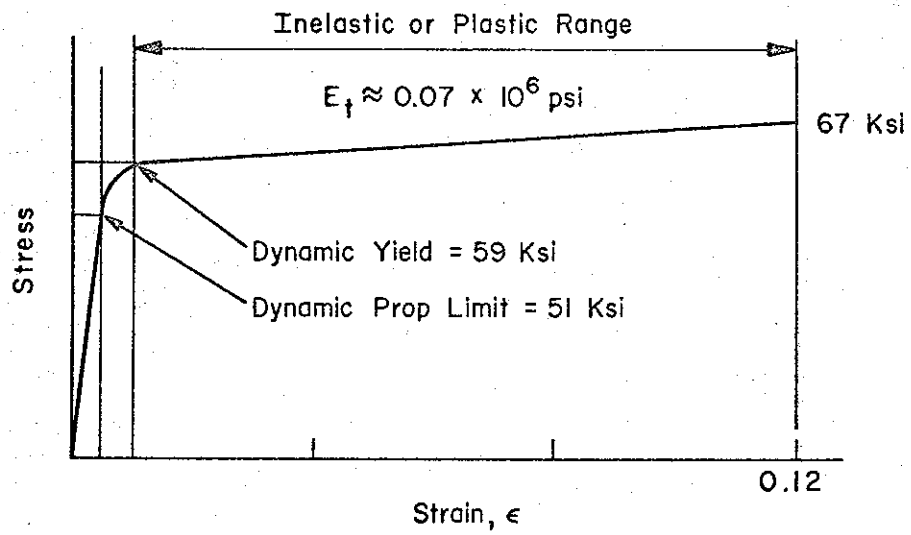

Figure 3.3 Idealized stress-strain curve of Aluminum 6061 T-6.

For short tubes, in which the ends are held circular but not otherwise constrained, Roark gives the following approximate formula for computing the first mode buckling stress,[2]

$$\sigma_{cr} = 0.81E\left(\frac{r}{\ell}\right)\left(\frac{h}{r}\right)\sqrt[4]{\left(\frac{1}{1-\nu^2}\right)^3\left(\frac{h}{r}\right)^2} \qquad (3.1)$$

where

σ_{cr} is the critical buckling stress,

E is the elastic modulus,

ν is Poisson's ratio,

h is the thickness,

r is the radius of the tube,

ℓ is the length between supports.

By analogy with results for long tubes given by Timoshenko, the higher mode critical stresses can be approximated by Equation (3. 2) below.[3]

$$\sigma_{cr} = \frac{(n^2-1)}{3.7} E\left(\frac{r}{\ell}\right)\left(\frac{h}{r}\right) \sqrt[4]{\left(\frac{1}{1-\nu^2}\right)^3 \left(\frac{h}{r}\right)^2} \quad (3.2)$$

where n = 2, 4, 6, etc.

Equations (3. 1) and (3. 2) are valid for determining the critical stresses up to the proportional limit. Elastic buckling in the nth mode may occur if the critical stress for that mode is less than the proportional limit.

Beyond the proportional limit, the buckling stresses can be computed from Equation (3. 2), if the elastic modulus is replaced by the tangent modulus E_t.[3, 4] It is important to note that in the plastic range, σ_{cr} and E_t are specified. Hence, for given values of r/ℓ and h/r, plastic or inelastic buckling will occur only for those values of n which satisfy Equation (3. 2).

Figure 3. 4 is a plot of the critical stresses for Sandia Test Cylinders A, as a function of radius $\frac{r}{h}$, (radius/thickness), for various modes, n. For simplicity, the stress in the inelastic range beyond the yield point has been assumed always to be equal to the yield stress. The $\frac{r}{h}$ ratios for the Test Cylinders A, of thicknesses h = 1/16-inch, 1/8-inch and 1/4-inch, are indicated in the figure.

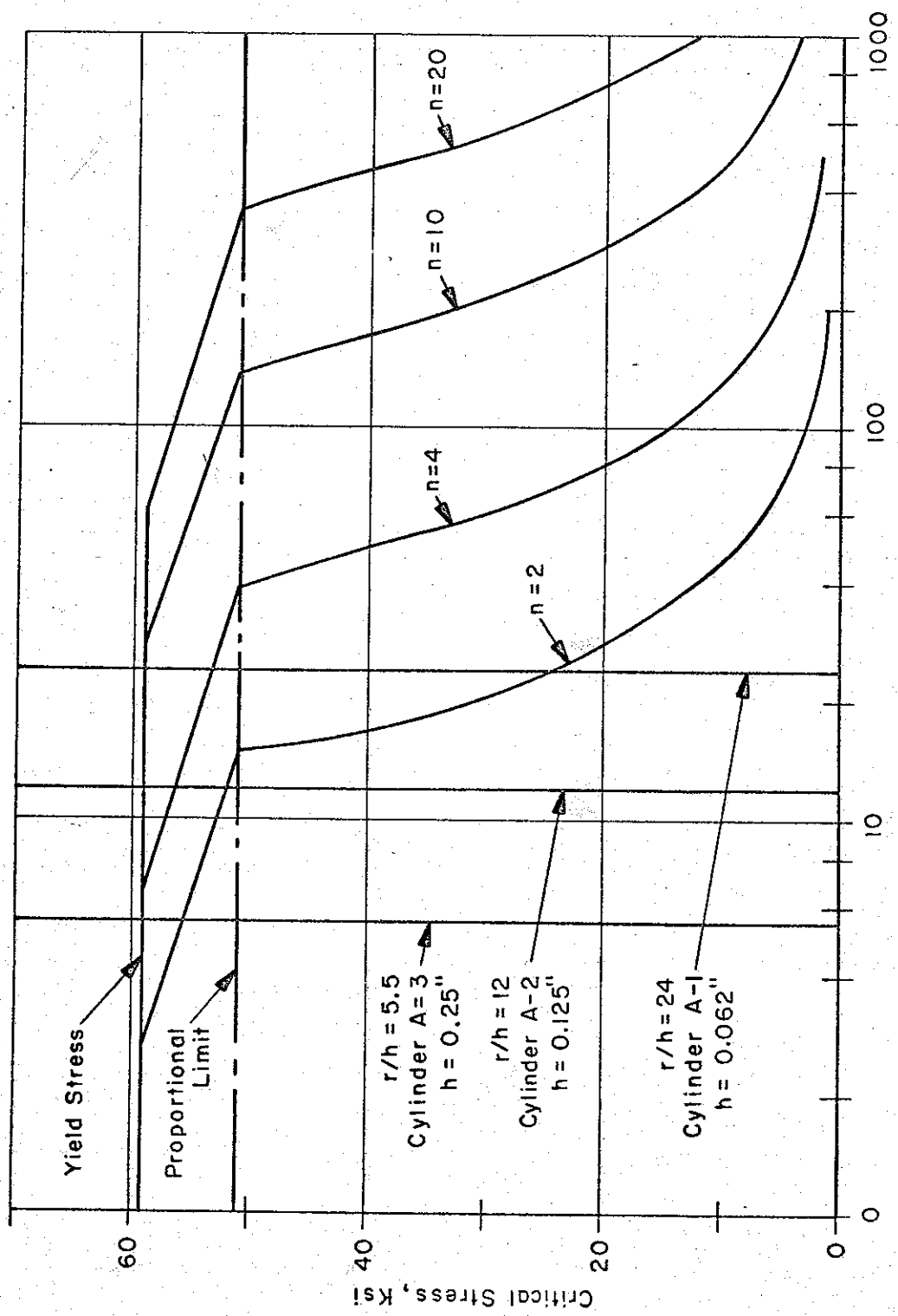

Figure 3.4 Critical buckling stress of "A" cylinders vs r/h for various modes.

From the data shown, it is apparent that elastic buckling could only occur in the 1/16-inch cylinder in the mode n = 2. Buckling between the proportional limit and the yield stress might occur in the 1/8-inch and 1/16-inch thick cylinders in the n = 4 mode, and in the 1/8-inch and 1/4-inch thick cylinders in the n = 2 mode. However, since, as already noted, the loading constraints are such as to preclude buckling in modes lower than approximately n = 8, it is unlikely that buckling will occur in any of the cylinders below the yield stress. The data in Figure 3.4 also indicates that inelastic or plastic buckling could occur after significant plastic deformation in the 1/16-inch cylinder in the n = 10 mode, in the 1/8-inch cylinder in the n = 6 mode, and in the 1/4-inch cylinder in the n = 2 mode. From the foregoing results, it appears likely that failure in all cylinders will involve significant uniform plastic deformation with some possibility of plastic, higher-mode buckling in the 1/8-inch and 1/16-inch thick cylinders.

3.3 ENERGIES AND PRESSURES TO PRODUCE FAILURE

The failure of all Sandia "A" cylinders has been shown to involve significant uniform, circumferential, plastic deformation. For the purpose of predicting the input energies and pressures required to produce failure, it will be assumed that uniform circumferential plastic deformation is the sole deformation and failure mode. End restraint effects will be neglected.

To simplify the failure analyses without significant loss of accuracy, the material characteristics will be approximated by that of a rigid-plastic material as shown in Figure 3.5. Failure will be assumed to occur when a strain of 12 percent is reached in Aluminum 6061 T-6.

3.3.1 Energy Required to Produce Failure. The energy required to produce failure is equal to the stored energy required to produce

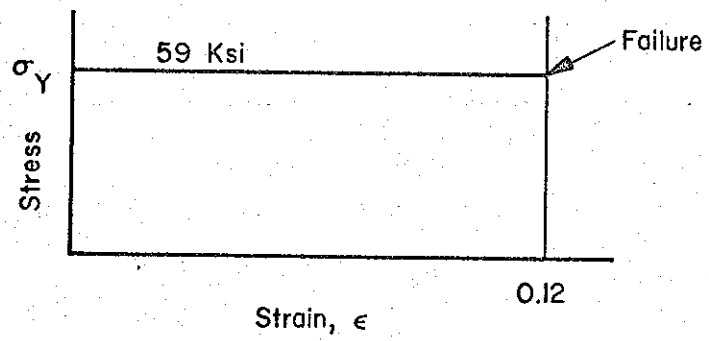

Figure 3.5 Rigid plastic material characteristics.

a 12 percent strain plus any kinetic energy possessed by the specimen when that failure strain is obtained. The failure energy per unit volume, $\frac{W}{V}$, is thus,

$$\frac{W}{V} = 1/2\,\gamma\,\dot{r}_f^2 + 0.12\,\sigma_y \qquad (3.3)$$

where

γ is the material density,

$\dot{r}_f$ is the radial velocity at time of failure,

σ_y is the yield stress,

V is the strained volume.

From Equation (3.3), the failure energy per unit length of specimen is

$$\frac{W}{\ell_o} = 2\pi r_o h_o \left\{1/2\,\gamma\,\dot{r}_f^2 + 0.12\,\sigma_y\right\} \qquad (3.4)$$

where

r_o is the initial radius,

h_o is the initial thickness,

ℓ_o is the initial loaded length.

An inspection of Equation (3. 4) shows that the value of the energy required to produce failure depends on the radial velocity at the time of failure, and it would seem that the values of W/ℓ_o which produce failure are unbounded. This, however, is not so. The value of $\dot{r}_f$ cannot be less than zero nor more than a critical radial velocity which, according to data given in Reference 5, is in the vicinity of 750 ft/sec. If it is assumed that the velocity of circumferential deformation cannot exceed the sonic velocity in the plastic range, where $E_T \simeq 0.07 \times 10^6$, it should be noted that the limiting radial velocity is about 220 ft/sec. For the purpose of establishing bounds on the required failure energy, it will be assumed that $0 \leq \dot{r}_f \leq 750$ ft/sec.

The two values of $\dot{r}_f$, when used in conjunction with Equations (3. 3) or (3. 4), determine upper and lower bounds for the required failure energy. If it is further assumed that only 7. 5 percent of the input energy is effectively used to deform the specimen, the upper and lower bounds of the input energy, per unit length of specimen, to produce failure are

Upper Bound: $\frac{W}{\ell_o} = 250,000\ h_o$ joules

Lower Bound: $\frac{W}{\ell_o} = 100,000\ h_o$ joules.

what length units??
Must be inches.

3.3.2 Pressure and Impulse to Produce Failure. The duration of loading, t_m, is sufficiently short, compared to the cylinder's response time, to consider the loading as an impulse which imparts a uniform initial radial velocity, $\dot{r}_o$, to the cylinder. The assumed magnetic pressure loading pulse is shown in Figure 3.6 and the loaded cylinder is shown in Figure 3.7.

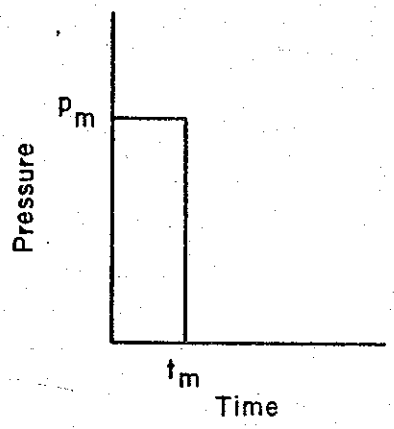

Figure 3.6 Assumed magnetic pressure loading pulse.

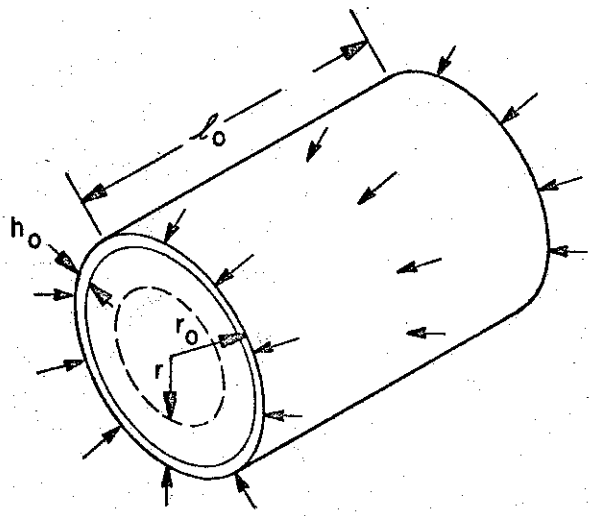

Figure 3.7 Pulse loaded cylinder.

The relation between the impulse characteristics p_m and t_m and the initial radial velocity is found from

$$\int_o^{t_m} F dt = \int_o^{v} M dv = M v_o$$

$$p_m \, 2\pi r_o \ell_o t_m = 2\pi r_o \ell_o h_o \gamma \dot{r}_o$$

which leads to,

$$\dot{r}_o = \frac{p_m t_m}{\gamma h_o} \qquad (3.5)$$

where

$\dot{r}_o$ is the initial radial velocity

p_m and t_m are impulse parameters.

Following this initial momentum transfer, uniform circumferential deformation proceeds. Assuming a perfectly plastic material, the deformation is retarded by the constant yield or plastic resistance of the cylinder. The equation describing this motion is

$$\gamma \ddot{r} = -\frac{\sigma_y}{r} \approx -\frac{\sigma_y}{r_o} \qquad (3.6)$$

For simplicity and without significant loss of accuracy, it has been assumed that the initial radius, r_o does not change appreciably (< 12 percent) during the deformation process. Note that Equation (3.6) with the initial condition, $\dot{r}\ (t = o) = \dot{r}_o$ is analogous to the equation of a body rising against gravity. The relation between the initial and final velocities can thus be written as

$$\dot{r}_o^2 = \dot{r}_f^2 + 2 \frac{\Delta r_f}{r_o} \frac{\sigma_y}{\gamma}$$

$$\dot{r}_o = \sqrt{\dot{r}_f^2 + 2 \frac{\Delta r_f}{r_o} \frac{\sigma_y}{\gamma}} \qquad (3.7)$$

where

Δr_f is the radial deformation at failure.

Combining Equations (3.6) and (3.7), and noting that the strain at failure $= \frac{\Delta r_f}{r_o} = 0.12$ which results in the following relation for the impulse per unit area, $p_m t_m$, to produce failure

$$p_m t_m = \gamma h_o \sqrt{\dot{r}_f^2 + \frac{\sigma_y}{4\gamma}} \qquad (3.8)$$

As in the case of the work required to produce failure, the impulse per unit area to produce failure depends upon the radial velocity at the time of failure. Again, upper and lower bounds on $p_m t_m$ can be established by considering the limiting cases; $\dot{r}_f = 0$, and $\dot{r}_f = 750$ ft/sec. These values of $\dot{r}_f$ yield the following upper and lower bounds for $p_m t_m$

Upper bound: $p_m t_m = 3 h_o \frac{\text{lb-sec}}{\text{in}^2}$

Lower bound: $p_m t_m = 2 h_o \frac{\text{lb-sec}}{\text{in}^2}$

where

h_o = initial material thickness, inches.

Further, for pulse durations of the order of 25 microseconds, the upper and lower bounds on the pressure required to produce failure are:

$$\text{Upper bound: } p_m = 12 \times 10^4 \, h_o \text{ lb/in}^2$$

$$\text{Lower bound: } p_m = 7.8 \times 10^4 \, h_o \text{ lb/in}^2$$

3.4 SUMMARY OF RESULTS

Using the equations that have been developed in the preceding sections, upper and lower bounds for the work and the pressure required to produce failure in the 1/16-inch, 1/8-inch and 1/4-inch thick Test Cylinders A have been calculated. These data are summarized in Table 3.1.

It should again be noted: that the tabulated input work assumes a 7.5 percent efficiency between the work that is effective in deforming the specimen and that stored in the capacitor bank: and that the pressure, p_m, is based on a pulse duration of 25 microseconds.

A qualitative comparison of the data in Table 1 with the limited experimental data that have been obtained indicates that there is general agreement between the predicted and experimental input work requirements; but that the predicted pressure range is somewhat low.

3.5 RECOMMENDATIONS FOR FUTURE EFFORTS

On the basis of the analytical work that has been performed, the following recommendations for additional study and investigation are made.

a. The cylinders tested to date have had r/h (radius/thickness) $\leq$ 24. These cylinders are not representative of full-scale cylindrical structures where r/h > 100, and they are not susceptible to buckling failures. Accordingly, it would be desirable to perform impulse

TABLE 3.1 WORK AND PRESSURE TO PRODUCE FAILURE

Cylinder	h_o (inches)	Input Work[1] / Specimen Unit Length		Pressure[2] p_m	
		Upper Bound	Lower Bound	Upper Bound	Lower Bound
A-1	1/16	15.5 kj/in.	6.2 kj/in.	7,500 psi	5,000 psi
A-2	1/8	31 kj/in.	12.5 kj/in.	15,000 psi	10,000 psi
A-3	1/4	62 kj/in.	25 kj/in.	30,000 psi	20,000 psi

[1]Assuming 7.5% efficiency

[2]Assuming t_m = 25 microseconds

tests on model cylinders with r/h > 100 where elastic and inelastic buckling would be the probable failure modes.

b. The experimental work should be extended to include the case of unsymmetrically loaded cylinders with a range of r/h values. Simple analytical models should be developed to estimate the loading parameters required to produce failure.

c. In addition to the work, pressure, etc., required to produce failure, the details of the deformation process are of considerable interest. These details include the time history of the deformation process, the loading parameters which just initiate yielding, etc. Experimental techniques which will permit the deformation process to be examined in detail should be studied and devised.

3.6 REFERENCES

1. Faupel, J. H., Engineering Design, p. 46; John Wiley and Sons, New York, N. Y., 1964.

2. Roark, R. J., Formulas for Stress and Strain, p. 318; McGraw-Hill, New York, N. Y., 1954.

3. Timoshenko, S., Theory of Elastic Stability, p. 450; McGraw-Hill, New York, N. Y., 1936.

4. Timoshenko, S., Strength of Materials, Vol. II, McGraw-Hill, New York, N. Y., 1956.

5. American Society of Tool and Manuf. Engineers, High Velocity Forming of Metals, p. 156; Prentice-Hall, Englewood Cliffs, N. J., 1964.

The general purpose of the impulsive load tests on aluminum cylinders was to demonstrate the impulsive load capabilities of pulsed magnetic fields and exploding films. These tests and the results are explained below.

4.1 MAGNETIC FIELD TESTS

4.1.1 Preparation.

4.1.1.1 Test Specimens. Five cylindrical test specimens of each of the three types specified on Sandia's drawings K38317 and K38330 were fabricated for testing. Gluing the phenolic sleeves to the aluminum cylinders was performed at EG&G's Bedford Potting Laboratory, following tests to determine the uniformity of the glue joints. The resulting test specimens were readied for the impulsive load tests after initial dry runs with extra samples.

4.1.1.2 Magnetic Impulse Testing Facility.

a. Capacitor Bank. A 33-kilojoule, 20-kilovolt capacitor bank with an internal inductance of 45×10^{-9} henries, resulting in a short circuit ringing frequency of 60 kilocycles, was activated and checked out; see Figure 4.1. The bank, part of EG&G's capital equipment, had been used extensively for magnetic metal forming investigations prior to the present tests. The application described here represents a logical extension of the existing facility and the information already obtained from its operation.

b. Pulsed Magnet Coils. A major requirement for the tests was the use of a pulsed magnet coil that was capable of sustaining the large electrical and mechanical impulses delivered by the 33-kilojoule bank. A previously developed multiple turn coil of relatively high efficiency was reconditioned and modified to accept the flux concentrator with the proper dimensions for the test specimens; see Figure 4.2. In

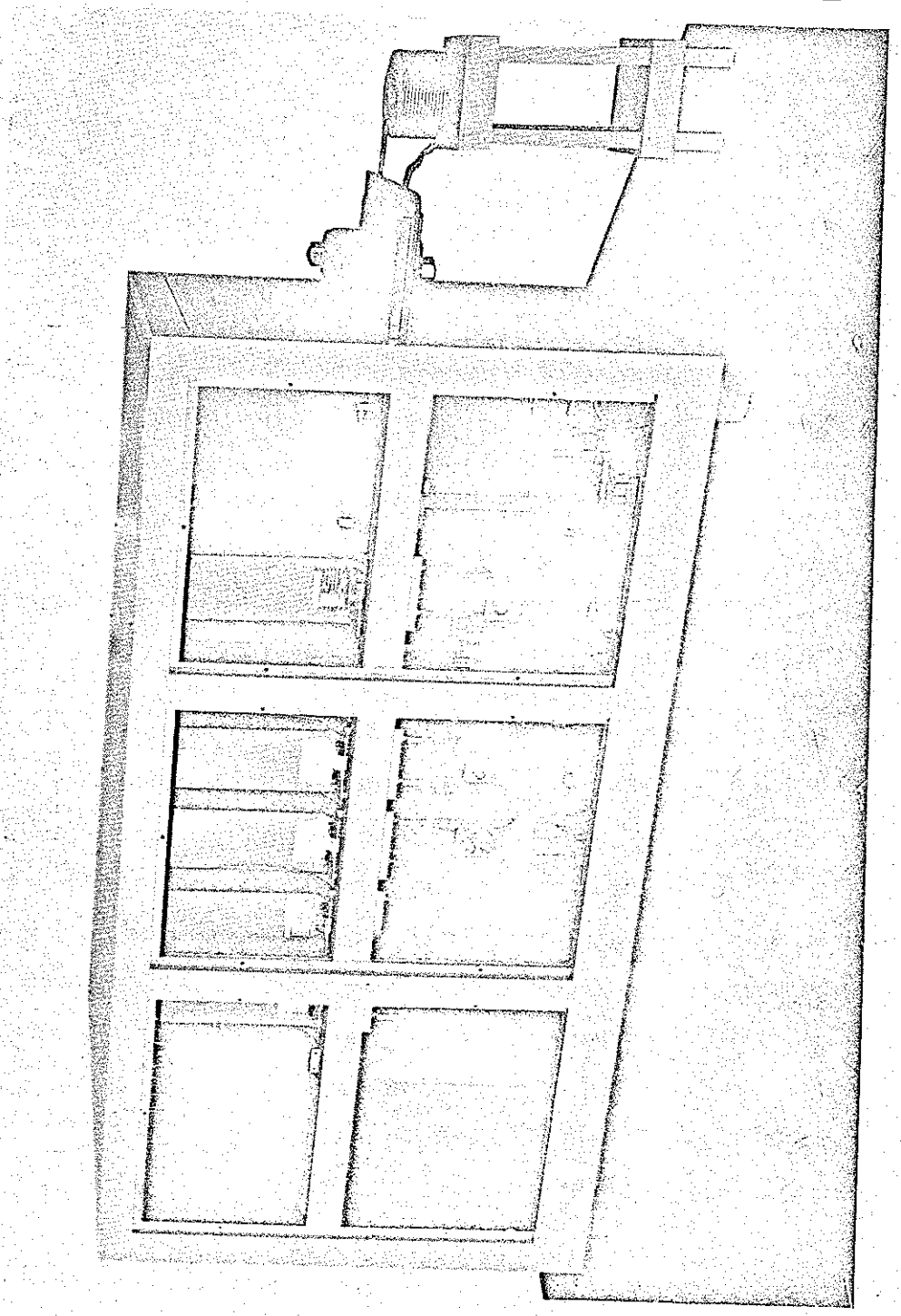

Figure 4.1 EG&G 33 kilojoule, 20 kv, 168 μF, 45 x 10^{-9} Henries capacitor bank.

addition, a single-turn berilium copper coil of identical dimensions to those of the flux concentrator was fabricated so that it could be mounted directly to the collector plate of the capacitor bank. This single-turn coil, although of lower magnetic efficiency, was capable of delivering pulses with a shorter duration than the multiturn unit. In addition, the simplicity of the single turn construction permitted a more accurate analysis of the circuit in comparison to the more complex analysis of the multiple turn coil with its associated coupling problems.

c. Exploding Wire Fuse. Normal operation of the capacitor bank with the inductive pulsed magnet resulted in a damped oscillatory discharge. Because it was anticipated that the multiple oscillations would be undesirable for analysis purposes, an exploding wire attachment as shown in Figure 4. 2 was devised to act as a fuse in series with the pulsed magnet in order to shut the current off after the first half cycle. Because the insertion of such a device adds inductance to the discharge circuit, the tests with the fuse were made with the higher efficiency multiple turn coil and flux concentrator in order to generate impulses of an acceptable magnitude on the test specimens.

d. Instrumentation. After experimenting with a variety of measuring techniques including current-measuring toroids, Rogowski loops, and high-voltage probes, instrumentation was limited to direct measurement of the voltage waveform at the flux concentrator. The waveforms were recorded by a Polaroid camera mounted on a Tektronix 507 oscilloscope. The "507", with its elimination of vertical amplifiers, allowed the recording of the signal with a minimum of pickup caused by the high transient dE/dt and dI/dt fields.

4. 1. 2 Test Procedure.

4. 1. 2. 1 Bare Aluminum Shells.

Figure 4.2 Experimental coil and workpiece with exploding wire attachment.

K38317-1: 0.065-inch wall
K38317-2: 0.125-inch wall
K38317-3: 0.25-inch wall

Each of the three-inch OD cylinders listed above were subjected, in succession, to the uniform radial impulses generated by the multiturn pulsed magnet, with the capacitor bank at full energy. Multiple runs were made with single and oscillatory impulses on the five sets of cylinders. Permanent deformation was accomplished on cylinders with the 0.065 and 0.125-inch thick walls. The waveshapes of the voltages taken at the flux concentrator were compared by means of multiple exposures to the waveshape obtained using the 0.25-inch wall tube, which showed no permanent deformation; see Figure 4.3. The deformation of the cylinders was measured and recorded. The previously deformed cylinders were then reinserted in the pulsed magnet, and the voltage waveforms recorded with the capacitor bank discharged at low energy to avoid further deformation of the cylinders. The resulting waveshapes were used to analyze the increase in voltage caused by the deformation on the original high-energy discharges.

Finally, a solid cylinder was fabricated with the same OD as the specified test sample. Comparison, by means of double exposure of the voltage waveforms of the 0.25-inch wall shell with the solid cylinder waveform, indicated elastic deformation of the 0.25-inch wall shell following the peak of the current pulse; see Figure 4.4.

4.1.2.2 Phenolic Aluminum Shells.

K38329-1: 0.125-inch phenolic/0.065-inch aluminum wall
K38329-2: 0.125-inch phenolic/0.125-inch aluminum wall
K38329-3: 0.125-inch phenolic/0.250-inch aluminum wall

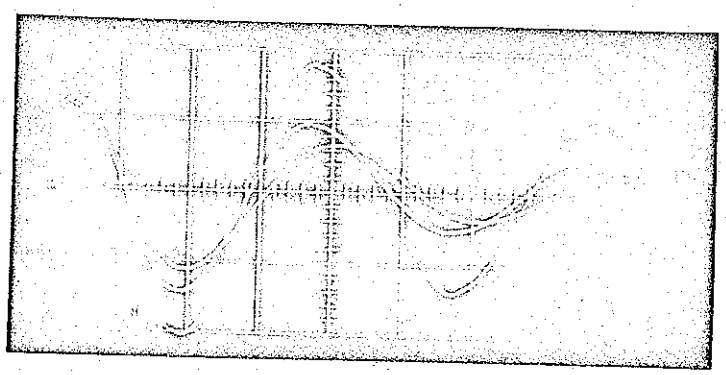

Sweep Speed 10 μsec/div Sensitivity 500 V/div

(Largest voltage oscillation is 0.065-inch wall thickness and smallest voltage oscillation is 0.25-inch wall thickness)

a. Ringing Impulse

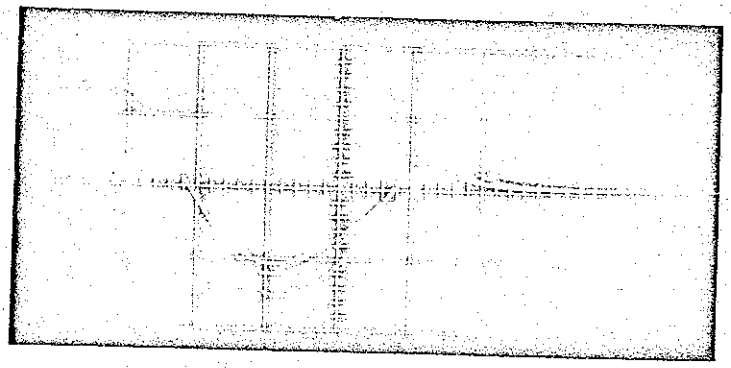

Sweep Speed 5 μsec/div Sensitivity 500 V/div

(Largest voltage oscillation is 0.065-inch wall thickness and smallest voltage oscillation is 0.25-inch wall thickness)

b. Single Impulse

Figure 4.3 Voltage vs time at flux concentrator with 3-inch OD cylinders of 0.065, 0.125 and 0.25-inch wall thickness. Capacitor bank discharged at 20 kv and 168 μF.

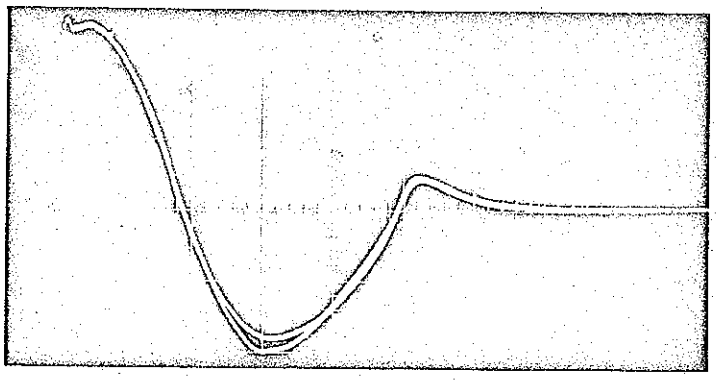

Sweep Speed 5 μsec/div Sensitivity 250 V/div

Figure 4.4 Voltage versus time at flux concentrator with 3-inch OD cylinders. Largest voltage oscillation is 0.065-inch wall thickness and smallest oscillation is solid cylinder.

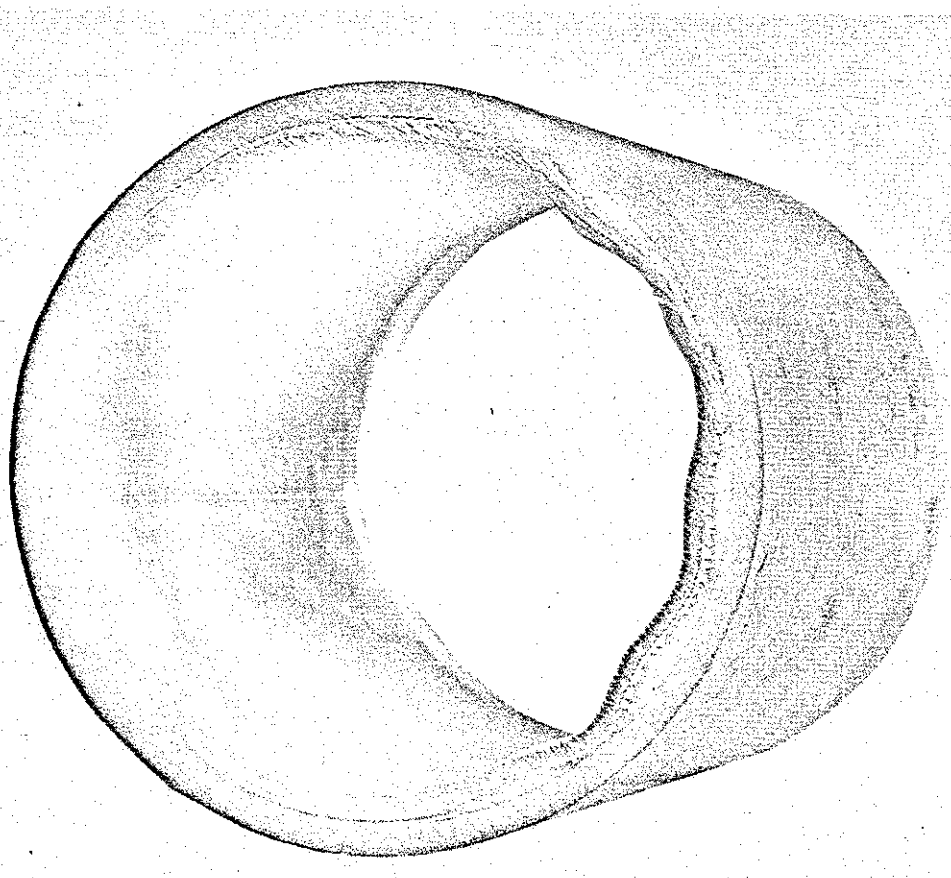

Figure 4.5 Deformed phenolic/aluminum cylinder.

Although uniform radial impulses were applied to the 0.065 and 0.125-inch aluminum wall tubes listed above, deformation was only observed on the 0.065-inch aluminum wall tube. Since this was anticipated because of the poor coupling caused by the space taken up by the phenolic wall tube, tests were carried no further than obtaining two samples of the minimum wall thickness 0.065 aluminum tube, (one sample shown in Figure 4.5).

4.1.3 Test Results. Initial conditions before impulsive loading are as follows:

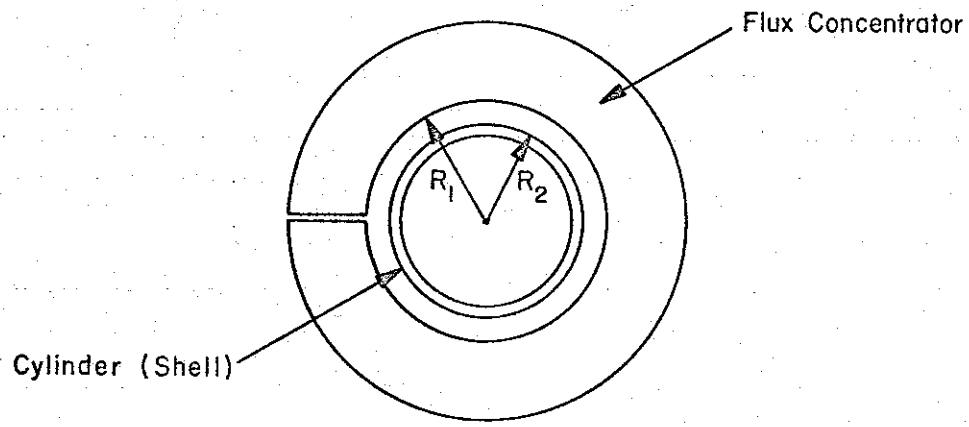

Figure 4.6 Diagram of initial conditions of cylinder and flux concentrator.

R_1, Inner radius of flux concentrator: 3.831 cm

L, Length of flux concentrator: 7.000 cm

V_1, Volume inside flux concentrator with no workpiece: 323 cm^3

R_2, Outer radius of all undeformed workpieces: 3.802 cm

V_2, Volume inside flux concentrator with undeformed workpiece: 4.70 cm^3

V_1/V_2, Ratio of volume with no workpiece to volume with workpiece: 69:1

$E_1/E_{2'}$ Ratio of voltage measured at concentrator with no workpiece to voltage on concentrator with undeformed workpiece: 7:1

Final conditions after impulse loading are as follows and as shown in Table 4.1 and Figure 4.7:

$R^1_{2'}$ Outer radius of deformed workpiece

$R_2 - R^1_{2'}$ Radial deformation

$V^1_2/V_{2'}$ Ratio of volume inside concentrator with deformed workpiece to volume inside concentrator with undeformed workpiece.

$E^1_2/E_{2'}$ Ratio of voltage at concentrator with deforming workpiece to voltage at concentrator with undeformed workpiece

$E''_2/E_{2'}$ Ratio of voltage at concentrator with undeformed workpiece

4.2 EXPLODING FILM TESTS

Five assemblies of a thin aluminum foil sandwiched within a cylindrical phenolic assembly which is, in turn, glued over an aluminum cylinder in accordance with Sandia drawing K-38329 were prepared. The purpose of this test was to determine the extent of the final deformation caused in the inner aluminum cylinder. The deformation was caused by exploding the thin aluminum foil by means of electrical energy obtained from a capacitor bank.

TABLE 4.1 FINAL CONDITIONS AFTER IMPULSE LOADING

	K38317-1 0.065-inch wall		K38317-2 0.125-inch wall		K38317-3 0.25-inch wall
	Ringing Discharge	Single Pulse	Ringing Discharge	Single Pulse	Single Pulse
R_2^1	3.365 cm	3.556 cm	3.734 cm	3.762 cm	---
$R_2 - R_2^1$	0.437 cm	0.246 cm	0.068 cm	0.040 cm	---
V_2^1/V_2	16:1 $\frac{cm^3}{cm^3}$	10:1 $\frac{cm^3}{cm^3}$	3.5:1 $\frac{cm^3}{cm^3}$	2.5:1 $\frac{cm^3}{cm^3}$	---
E_2^1/E_2	3:1 $\frac{v}{v}$	2:1 $\frac{v}{v}$	---	1.2:1 $\frac{v}{v}$	---
E_2''/E_2	3:1 $\frac{v}{v}$	2:1 $\frac{v}{v}$	1.35:1 $\frac{v}{v}$	1.2:1 $\frac{v}{v}$	1.12:1 $\frac{v}{v}$

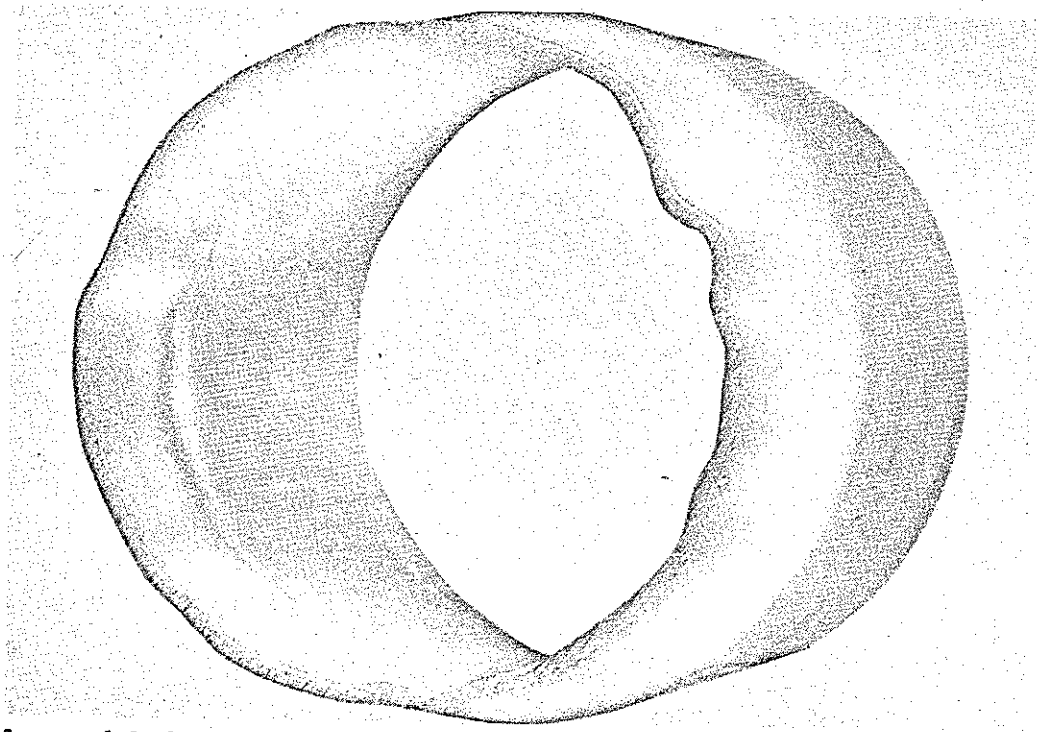

a. Deformed 0.065-inch wall thickness cylinder subjected to ringing impulse.

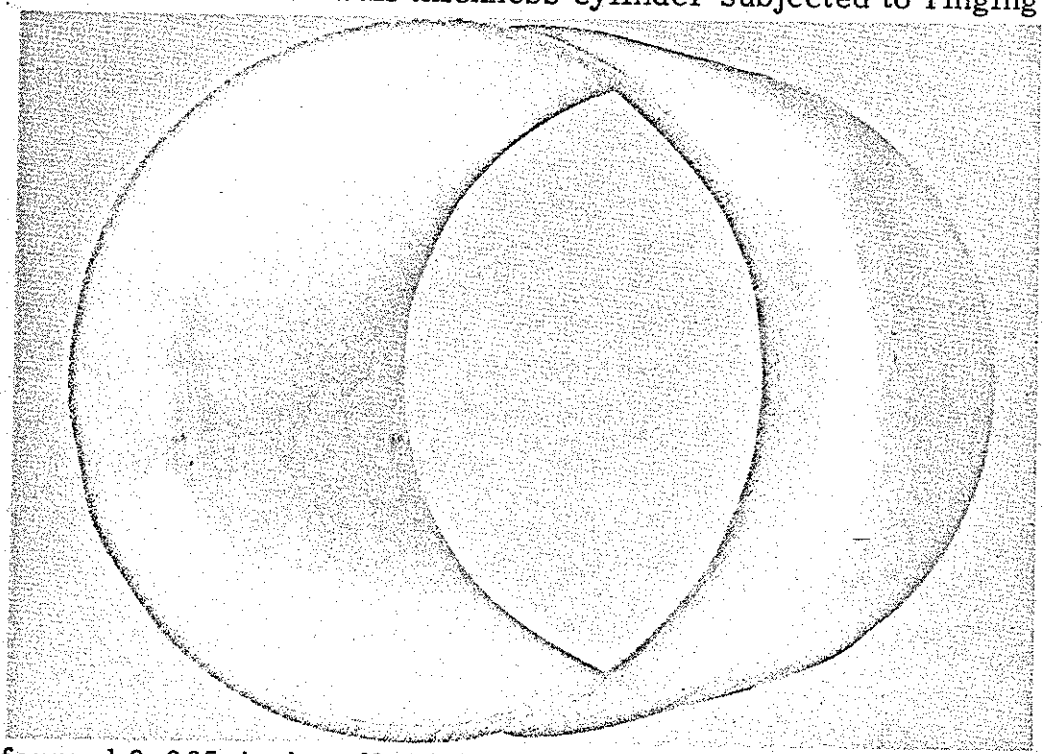

b. Deformed 0.065-inch wall thickness cylinder subjected to single impulse.

Figure 4.7 Deformed cylinders after impulse loading.

Five tests were performed and produced negative results. In all cases the foil did not explode homogeneously and the damage to the cylindrical assemblies was limited to localized damage to the outer phenolic tube.

Five new assemblies have been prepared and will be tested in the near future. These new assemblies are a significant departure from the previous assemblies, and the results of the tests will be described in the next progress report. Emphasis has been placed on obtaining a homogeneous discharge in the foil.

4.2.1 Preparation.

4.2.1.1 The Cylindrical Structure. The structure consisted of a 1/8-inch thick aluminum tube, 11 inches long, and having a 4-inch outside diameter. A 1/8-inch phenolic tube is telescoped and glued to the outside diameter of the aluminum tube. On the outside diameter of the phenolic tube, an aluminum film of approximately 1 microinch is vacuum deposited, and another 1/8-inch phenolic tube is telescoped and glued to the outside diameter of the aluminum film.

Three of these assemblies had a fully symmetrical (360 degrees) aluminum film coating, while the other two had a film coating over half the circumference (180 degrees).

The aluminum tube and the aluminum foil are connected electrically at the end of the tube, thus making a low-inductance exploding foil load.

The two ends of the aluminum tubing are covered with two 1/2-inch thick aluminum plugs that are held in place by a half-inch threaded rod through the axis of the assembly

4.2.1.2 The Electrical Circuit. A three thousand joule capacitor (3.75 microfarads at 40 kv) is discharged into the exploding foil load through a high-current switch. The shorted ringing frequency of the

complete system is 0.33 megacycle (75×10^{-9} Henry),
The selection of the custom built compacitor and the overall coaxial geometry make possible the high ringing frequency of the system.

4.2.1.3 Diagnostic Equipment.

a. Load Current. A four-turn coil is inserted in the coaxial space between the capacitor and the spark gap. By means of a 20-microsecond time constant RC network, the pick-up coil signal, di/dt, is integrated, and the resulting trace, i, is displayed on a Tektronics scope. This signal can be used to calculate the energy deposited in the exploding foil.

b. Voltage Measurement. A resistive voltage divider is used to measure the residual potential in the capacitor after the discharge has taken place. This residual potential can be used to correct the energy calculation in paragraph 4.2.1.3a.

c. The 6-Frame Kerr Cell Camera. An independently pulsed light source is used to back-light the aluminum-phenolic assembly. An 8-inch diameter lens collimates the beam from the light source to the Kerr Cell lens. The Kerr Cell Camera was used to record the debris motion of the exploding outer phenolic tube and to give a measurement of the shock wave. The shock-wave front film record can be used to calculate the shock velocity. The frames of the Kerr Cell can be spaced from 1.2 up to 50 microseconds apart. The Kerr Cell exposure time is approximately 0.25 microsecond.

d. The Time Sequence. The operator triggers the external back-light source. Some of this back light falls on a photo cell which triggers the experiment as well as the diagnostic equipment with appropriate delays for each. The event and the first Kerr Cell frame are delayed until the external light source reaches peak intensity with the event preceding the first Kerr Cell frame by one microsecond. This corresponds to the first peak current pulse.

4.2.2 The Experiment.

4.2.2.1 Test 1. This test assembly had a 360-degree aluminum foil of one microinch thickness. The phenolic tube containing the explosion was 1/8-inch thick. The discharge on this shot followed a single path of the lightning-stroke variety on the side facing the Kerr Cell Camera. In fact, frames 2 and 6 of Figure 4.8 distinctly show this path. Upon visual examination of the exploding foil assembly, it was found that most of the aluminum foil was unmarked except along the path of the discharge. Also, the outer phenolic tube broke up in clean large pieces except along the discharge path where the carbonized debris was granular. Along the discharge path, the aluminum tube was pressed in an oblong cross-section by only 0.015 inch. The signal from the current pickup was extremely small indicating that the foil behaved resistively. It is estimated that the exploding foil had a resistance of approximately 5×10^2 ohms along the discharge path for at least the first 15 microseconds. The lack of discharge homogeniety is tentatively attributed to the mixing of the glue with the aluminum film and the total lack of air space in the region of the explosion.

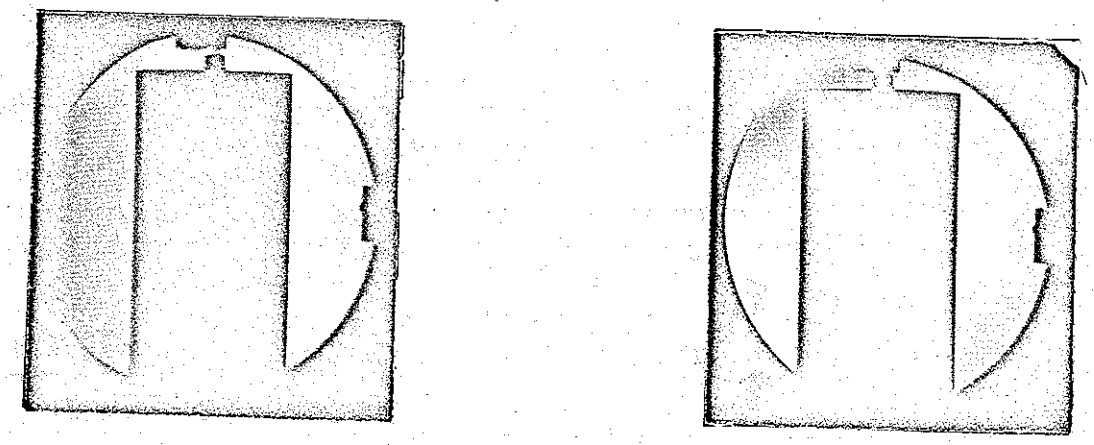

F2 F6

Figure 4.8 Kerr Cell camera record of the exploding assembly.

Another interesting observation is the lack of damage done to the inner cylindrical structure (aluminum and phenolic tube) while the outer phenolic tube was completely blown off. In the past, a fully contained single path discharge at the same input energy level deformed a brass tube of similar dimensions by approximately 1/2-inch buckling. The reason for the different amount of damage done in the two situations is being investigated.

Most of the effort at the present time is devoted to obtaining a homogeneous discharge using an experimental assembly.

4.2.2.2 The "Experimental Assembly". This experimental test assembly consists of a solid aluminum cylinder covered with ten layers of 0.010-inch mylar. The aluminum exploding foil was secured on the surface of the mylar with scotch tape. For various shots, the number of layers of mylar used to contain the exploding foil were varied. Through these tests, it was found that two layers of 0.010-inch mylar resulted in a reasonably homogeneous explosion of the foil. For this reason, the outer phenolic tubes of the original exploding foil assemblies were turned down to a 0.020-inch thickness.

4.2.2.3 Tests 2, 3, 4, and 5. Two of the assemblies had a full circumferential exploding foil while the other two had the exploding foil for only 180 degrees of the tube circumference.

All four of these discharges were also non-homogeneous. The discharge again occurred through a single line path. The Kerr Cell Camera indicates that the thin outer phenolic tube broke up in the first 2 to 3 microseconds, thus permitting ionization of the air along the discharge path. Indeed, the current traces indicated a peak value of about 10^5 amps. No damage or deformation was observed on the aluminum-phenolic inner assembly.

4.2.3 Conclusions. In the past our ability to homogeneously explode a cylindrical foil of approximately one microinch with approximately 4 to 5-inch diameter and 10 to 20 inches long was based on the gaseous space between the exploding foil and the outer cylindrical wall. When this space was properly chosen, it would result in a critically damped discharge with the microinch foil acting like the plasma material. For the dimensions used and the 3000 joules of energy available, this space was typically 0.015 to 0.050 inch, which was large enough to lower the peak pressure generated by the discharge. For this reason, this approach could not be used directly in the present experiment. Instead, the approach used in the present assembly had the exploding foil completely imbedded inside the two phenolic tubes by means of glue. Such an assembly would produce high pressures in the first microsecond and become an ideal tool for the study of energy deposition in the internal layers of the materials and geometries selected if the discharge could be made homogeneous. The non-homogeniety observed in the five shots reduces considerably the value of this approach. We are presently investigating methods for obtaining the required homogeneous discharge. One approach being followed is to increase the thickness of the foil and at the same time reduce the foil area to maintain a reasonably high energy per unit volume ratio. Should this approach be fruitful, it will be necessary to increase the stored energy on the capacitor bank in order to homogeneously explode foils of the desired area.